Structure−Function Relationships in Helix-Bundle Channels Probed via Total Chemical Synthesis of Alamethicin Dimers: Effects of a Gln^7 to Asn^7 Mutation†

Dominic C. J. Jaikaran,‡,§ Philip C. Biggin,§,|| Holger Wenschuh,⊥ Mark S. P. Sansom,|| and G. Andrew Woolley*,‡

Department of Chemistry, University of Toronto, 80 St. George Street, Toronto M5S 3H6, Canada, Max-Planck-Institute for Infection Biology, Monbijoustrasse 2, 10117 Berlin, Germany, Institute of Molecular Pharmacology, Kowalke Strasse 4, 10315 Berlin, Germany, and Laboratory of Molecular Biophysics, University of Oxford, South Parks Road, Oxford OX1 3QU, U.K.

Received July 3, 1997; Revised Manuscript Received August 21, 1997⊗

ABSTRACT: Alamethicin channels are prototypical helix bundles that may serve as tractable models for more complex protein ion channels. Solid-phase peptide synthesis of alamethicin analogues using FMOC-amino acid fluorides followed by chemical dimerization of these peptides facilitates structure−function studies of particular channel states in bilayer membranes. State 3 in particular, tentatively assigned to a hexameric helix bundle, is sufficiently long-lived that current−voltage measurements can be made during the lifetime of an individual channel opening. Molecular models of hexameric helix bundles, generated using restrained molecular dynamics with simulated annealing, indicate that a $Gln^7 \rightarrow Asn^7$ (Q7 → N7) mutation will increase channel diameter locally. Experimentally, the conductance of state 3 of the N7−alm channel is found to be larger than that of the Q7−alm channel when ion flow is in the usual direction (cations entering the C-terminal end of the channel). When ion flow is in the opposite direction, no difference in the conductances of state 3 of Q7 and state 3 of N7 channels is observed. These results indicate that the effect of a change in pore diameter at position 7 is dependent on the magnitude of other barriers to permeation and that these barriers are voltage-dependent.

Alamethicin and related peptides have been studied intensively as model ion channels (*1*−*5*). These peptides self-assemble in membranes to form ion-conducting helix bundles. Since some important ion channel proteins also appear to be helix bundles (*6*), the alamethicin system is a relevant model. A molecular understanding of ion transport in this model might help us to understand the permeability properties of more complex protein channels. In addition, such an understanding may facilitate the design of channel-forming peptides with specific properties (*e.g.* ion selectivity) (*7*).

While a wide range of structural, biophysical, and computational studies have been reported on alamethicin systems, two factors have hampered systematic structure−activity studies. The first is the difficulty of chemical synthesis of peptides containing large numbers of aminoisobutyric acid (Aib)[1] residues. To circumvent this problem, Molle et al., for example, have resorted to complete replacement of all eight Aib residues of alamethicin by Leu for structure−activity studies (*8*−*15*). These des-Aib-Leu peptides show properties similar to those of alamethicin, but the channels formed appear to be significantly less stable than those formed by the native peptide (*12*). The recent introduction of the acid-fluoride technique has now made possible automated solid-phase peptide synthesis of alamethicin (and other multiple-Aib-containing peptides) (*16*−*19*).

The second difficulty that has hampered systematic structure−activity studies is the fact that channel self-assembly leads to a wide range of conducting structures with different molecularities. Structure−function studies would be more easily interpreted if they occurred within the context of one predominant conducting structure rather than within a family of structures. We have recently demonstrated that covalent dimerization of alamethicin peptides leads to selective stabilization of particular conducting states (*20*). Dimerization does not completely solve the problem of multiple conductance states; it does, however, result in a pattern of stabilization that enables one to recognize states that are likely to be of the same molecularity. Although the absolute molecularity of any particular state has not been unambiguously determined, the comparison of channel mutants that each have the same molecularity can still provide useful structure−activity data.

This study makes use of both these advances in examining the effect of a $Gln^7 \rightarrow Asn^7$ (Q7 → N7) mutation on the properties of particular conducting structures. This mutation has been studied in the context of the des-Aib-Leu peptides channels by Molle et al. (*8*) and was found to decrease channel conductance under steady-state constant-voltage

† This work has been supported by the Canadian Cystic Fibrosis Foundation, NSERC Canada, and the Wellcome Trust.

* To whom correspondence should be addressed.
‡ University of Toronto.
§ These authors contributed equally to this work.
|| University of Oxford.
⊥ Max-Planck-Institute for Infection Biology and Institute of Molecular Pharmacology.

⊗ Abstract published in *Advance ACS Abstracts,* October 1, 1997.

[1] Abbreviations: alm, alamethicin; Asn, asparagine; BAPHDA, bis-(*N*-3-aminopropyl)-1,7-heptanediamide; BES, *N*,*N*-bis(2-hydroxyethyl)-2-aminoethanesulfonic acid; DAST, (diethylamino)sulfur trifluoride; DCM, dichloromethane; DIEA, diisopropylethylamine; DMF, dimethylformamide; EDTA, ethylenediaminetetraacetic acid; ESI-MS, electrospray ionization mass spectrometry; Fmoc, 9-fluorenylmethyloxycarbonyl; Gln, glutamine; HATU, *O*-(7-azabenzotriazol-1-yl)-*N*,*N*,*N*′,*N*′-tetramethyluronium hexafluorophosphate; HPLC, high-performance liquid chromatography; *I*−*V*, current−voltage; SA/MD, simulated annealing via molecular dynamics; MeOH, methanol; NMM, *N*-methylmorpholine; PAPDA, pimelic acid piperazine diamide; SPPS, solid-phase peptide synthesis; TFA, trifluoroacetic acid.

S0006-2960(97)01613-9 CCC: $14.00 © 1997 American Chemical Society

conditions. Since, *prima facie*, the shorter side chain of Asn should lead to a wider pore and so to a higher conductance, we were prompted to examine the same mutation in the native alamethicin system where experimental results and molecular models could be directly compared. Chemical synthesis and dimerization of both Q7−alm and N7−alm gave peptides that formed channels in a manner qualitatively similar to that observed previously with dimeric native alamethicin (alm−BAPHDA) (*20*). Current levels of dimer channels matched those of channels formed by the corresponding Q7 and N7 monomers, indicating that the linkers do not substantially affect the pore structure of the channel. In both cases, dimerization led to selective stabilization of alternate conductance levels that are believed to arise from structures of even-numbered molecularity. One structure in particular, which by analogy with previous work we tentatively assign as the hexamer (three dimers), forms reproducibly and has a lifetime sufficient to permit a measurement of single-channel current−voltage ($I-V$) relationships.

The single-channel $I-V$ curve of the Q7-alm dimer can be superimposed on that of native dimeric alm (alm−BAPHDA). The N7−alm dimer channel gives an $I-V$ curve with a similar shape, but the currents are greater in magnitude with positive voltages than those of the Q7−alm dimer. At negative voltages, the magnitudes of the currents of the N7− and Q7−alm dimers are approximately equal. These results are discussed in the context of molecular models of hexameric Q7 and N7 pores.

MATERIALS AND METHODS

Synthesis of Q7−Alamethicin Acid and N7−Alamethicin Acid. Assembly of the alamethicin acid analogues was performed via stepwise solid-phase synthesis on an ACT 348 multiple-peptide synthesizer (Advanced ChemTech, Louisville, KY). Initially, *o*-chlorotrityl resin (NovaBiochem, Bad Soden, Germany, resin capacity of 1.5 mmol/g) was loaded manually with Fmoc-Phe-OH (3 equiv of Fmoc-Phe-OH, 6 equiv of DIEA, and DCM) for 2 h. Stepwise synthesis was achieved with isolated Fmoc-protected amino acid fluorides [single couplings, 30 min, 4 equiv of Fmoc-AA-F and 4 equiv of DIEA (0.3 M) in DMF]. Fmoc-amino acid fluorides were prepared with DAST as described recently (*21*). The Fmoc protecting groups were deblocked with 25% piperidine/DMF for 15 min, and the final N-terminal acetylation was achieved with a mixture of acetic anhydride/DIEA/DMF (1:2:7) for 30 min. Peptide resin cleavage was performed with a solution consisting of 2% triisopropylsilane and 5% water in 50% DCM/TFA for 50 min. After precipitation in ether, peptides were purified by preparative HPLC (Polyenecap A300 column, 4.6 × 125 mm, linear gradient; eluant A, 0.1% TFA in water; eluant B, 0.1% TFA in 80% acetonitrile/20% water) and analyzed by HPLC and ESI-MS. The purity by HPLC was >95%. ESI-MS: calcd for Q7-alm-acid 1978.4 $[M + H]^+$, found 1977.2 $[M + H]^+$; calcd for N7-alm-acid 1964.3 $[M + H]^+$, found 1963.8 $[M + H]^+$. Prior to dimerization, these peptides were passed through another preparative HPLC column (Zorbax SB-C18 column, 9.4 × 250 mm, 92:8 MeOH/H_2O, 1.5 mL/min) to remove residual TFA.

Synthesis of Q7−Alm and N7−Alm Dimers. The linker BAPHDA [bis(*N*-3-aminopropyl)-1,7-heptanediamide] was synthesized as described previously (*20*). Syntheses of Q7 and N7 dimers were carried out in the same manner, so only the synthesis of the Q7 dimer is described in detail; 2 mg (1 μmol) of Q7−alm acid (purified by HPLC), 0.76 mg (2 μmol) of HATU (Perseptive Biosystems, Inc.), and 0.404 mg (4 μmol) of NMM were dissolved in 1 mL of DMF. The mixture was cooled in ice/water for 15 min. Then, 0.118 mg (0.44 μmol) of BAPHDA was added dropwise over 10 min. The reaction mixture was stirred on ice for 1 h and then at room temperature overnight. TLC (65:25:4 $CHCl_3$/MeOH/H_2O): Q7−alm monomer R_f 0.15, Q7−alm dimer R_f 0.45, N7−alm monomer R_f 0.18, N7−alm dimer R_f 0.42. The solvent was evaporated under high vacuum, and the residue was redissolved in MeOH. The dimer product was then separated from the reaction mixture and purified using analytical HPLC (Q7 dimer, Zorbax RxC8 column with 90:10 MeOH/H_2O at 1 mL/min, $t_R = 11.0$ min; N7 dimer and Q7 dimer, Zorbax SBC18 column with 88:12 MeOH/H_2O, $t_R = 28$ min). Dimers eluted with significantly longer retention times than monomers as observed previously when native alamethicin was cross-linked (*20*). HPLC-purified dimers were characterized using ESI-MS (Figure 2): calcd for the Q7−alm dimer ($C_{197}H_{322}N_{50}O_{50}$) 4191, found 4191; calcd for the N7−alm dimer ($C_{195}H_{318}N_{50}O_{50}$) 4163, found 4162.

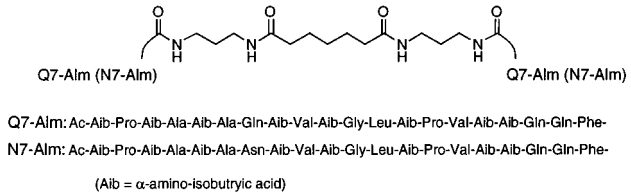

FIGURE 1: Chemical structures of the alamethicin dimers. The C-terminal residue of each peptide is a normal phenylalanine (Phe) residue (as opposed to the phenylalaninol of natural alamethicin). The carboxyl group of this Phe forms an amide bond with one end of the BAPHDA linker as shown.

Single-Channel Measurements. HPLC-purified peptides (~0.01 μM in MeOH) were added to both sides of membranes formed from diphytanoylphosphatidylcholine/decane (50 mg/mL) using established techniques (*22*). A 1 M potassium chloride solution, buffered with BES (5 mM) to pH 6.8, was used throughout, and all measurements were made at 23 °C (±2 °C). Currents were measured, and the voltage was set using an Axopatch 1D patch-clamp amplifier (Axon Instruments) controlled by Synapse (Synergistic Research Systems) software. Data were filtered at either 5 or 10 kHz, sampled at 2 times the filter frequency, stored directly to disk, and analyzed using Synapse and Igor (Wavemetrics, Inc.) software. Raw continuous data were smoothed once using a Gaussian filter in the data analysis program Igor (binomial setting 1; Wavemetrics, Inc.).

Single-channel current−voltage ($I-V$) curves were obtained using the following voltage-clamp protocol: a step from 0 to 200 mV, holding at 200 mV for 50−500 ms, then a ramp to −200 mV over the course of 10−50 ms, followed by a return to 0 mV for several seconds. Capacitive currents obtained when no channel opened were subtracted from currents obtained with a single channel open during the ramp. Data shown are for individual ramps. Repeat ramps (generally 5−25) gave $I-V$ curves that could be superimposed on those shown. $I-V$ curves were obtained for channels opening at −200 mV by applying an inverted protocol (*i.e.* a ramp from −200 to 200 mV).

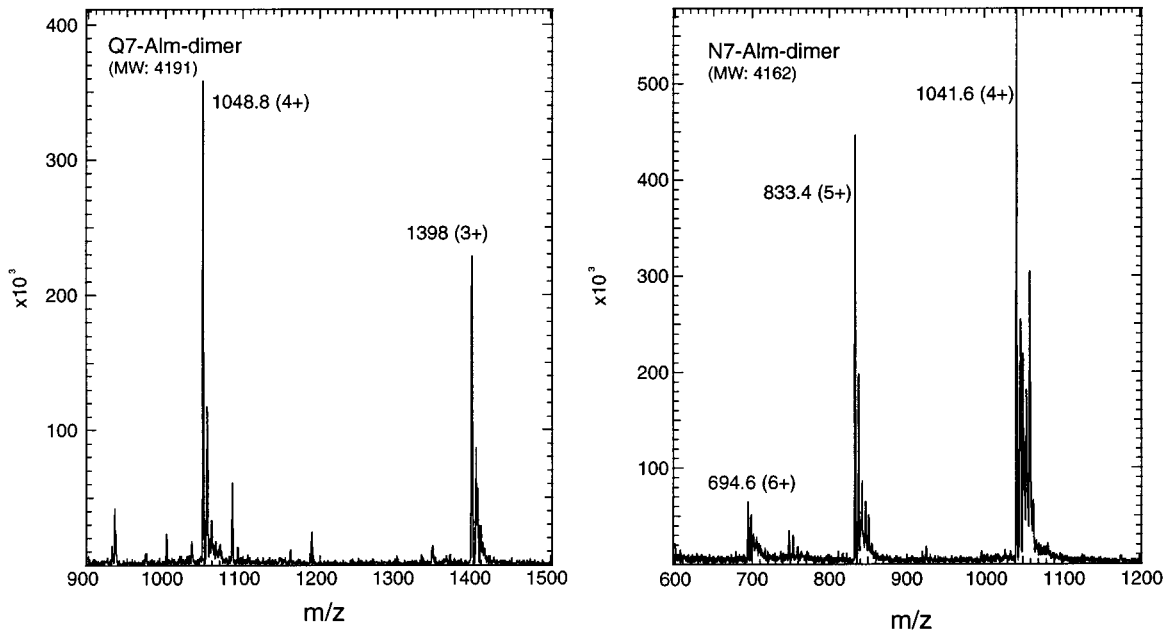

FIGURE 2: Electrospray mass spectra of the Q7−alm dimer and the N7−alm dimer. A range of Na adducts is observed for each charged state. The average observed mass of each dimer is indicated.

MOLECULAR MODELING

(1) Programs. In vacuo molecular dynamics (MD) simulations and model building were carried out using Xplor V3.1 (*23*) with the CHARMm PARAM19 (*24*) parameter set. Only H atoms attached to polar groups were represented explicitly; apolar groups were represented by extended atoms. MD simulations in the presence of water were performed using CHARMm v23 (*24*). Display and examination of models was carried out using Quanta V4.0 (Biosym-Molecular Simulations), and diagrams of structures were drawn using Molscript (*25*). Pore dimensions were calculated using HOLE (*26*, *27*). MD simulations were performed on DEC Alpha workstations, and all other calculations were carried out on Silicon Graphics workstations.

(2) Simulated Annealing via Restrained Molecular Dynamics. Hexameric bundles of the Q7 and N7 analogues were constructed by "mutating" alm−BAPHDA bundles that were constructed by simulated annealing via restrained molecular dynamics (SA/MD). This method has been described in full by You et al. (*20*) and is similar to that employed by Nilges and Brunger (*28*, *29*) to predict the experimental structure of GCN4 helix dimers. The applications of the method to modeling both single-transmembrane helixes (*30*−*32*) and bundles of transmembrane helixes (*20*, *33*−*37*) have been described in detail. Briefly, the method starts from a Cα template and includes distance restraints during the MD simulations in the final stage of the procedure. Intrahelical restraints used were intended to mimic the presence of α-helical hydrogen bonds and acted between the CO and NH groups of the peptide backbone. Interhelical restraints were used to direct the packing of the bundle.

(3) Assumptions Underlying the Models. When a channel composed of amphipathic helixes is constructed, several assumptions have to be made (*34*): (a) the number of helixes in the bundle, (b) whether the helixes are parallel or antiparallel to one another, (c) the orientation of the helixes (by rotation about the helix long axis) relative to the center of the pore, and (d) in the case of kinked helixes such as that of alamethicin whether the N- or C-terminal helixes are close-packed within the bundle. The first assumption is that the bundle is comprised of three dimers (corresponding to six alamethicin monomers). The assumption that neighboring helixes are parallel, rather than antiparallel, is consistent with current models of alamethicin channel structure and gating (see below). We further assume that polar residues are oriented toward the channel lumen and that the N-terminal ends are close-packed (*20*, *33*).

(4) Modeling of the Q7−Alm Dimer Bundles. The Q7 bundles were made by simply mutating the linker in the alm−BAPHDA bundles (*20*) to the linker shown in Figure 1 using the molecular editor in Quanta. CHARMm topology patches were written to represent the covalent structure of the linker. This mutated structure was then subjected to four stages of energy minimization. In the first stage, the rest of the peptide was constrained and only the linker residues were allowed to move. In the second stage, only harmonic restraints were applied to the protein backbone. In the third stage, the only restraints were on the Cα atoms of the protein, and in the final stage, there were no restraints.

This final minimized structure was then solvated using protocols based on those described previously (*38*, *39*). The water model employed was a TIP3P three-site model (*40*) with partial charges qO = −0.834 and qH = 0.417, modified as in the CHARMm parameter set. The Q7 bundle (comprising three dimers) was solvated using a pre-equilibrated cylinder (length of 60 Å, radius of 7 Å) of water molecules. Water molecules from this cylinder were selected so that the central pore and the cap regions at either mouth of the pore were solvated but that no such water molecules were present on the bilayer-exposed surface of the bundle.

Prior to molecular dynamics, this solvated structure was minimized with a four-stage process: (a) 1000 cycles of adopted basis Newton Raphson (ABNR) with the protein atoms fixed, (b) 1000 cycles of ABNR with the protein backbone atoms restrained, (c) 1000 cycles of ABNR with weak restraints on the protein Cα atoms only, and (d) 1000 cycles of ABNR with no positional restraints. Molecular dynamics was then run with a 1 fs time step. The system

was heated from 0 to 300 K in 6 ps (5 K, 0.1 ps steps) and equilibrated for 9 ps at 300 K by rescaling the atomic velocities every 0.1 ps. The production stage was 85 ps, giving a total simulation time of 100 ps. Nonbonded interactions were truncated using a shift function (*24*) with a cutoff of 13.0 Å.

During the simulation, a number of restraints were applied: (a) a cylindrical restraining potential on the waters (*38*, *39*) to prevent "evaporation" from the mouths of the pore, (b) intrahelix restraints (between NH and CO groups) to maintain the peptides in an α-helical conformation, (c) interhelix restraints (between the geometrical centers of adjacent helixes in the bundle) to hold together the helix bundle (*34*, *35*), and (d) a "bilayer" potential, based on residue-by-residue hydrophobicities (*41*−*43*), to mimic the embedding of the helix bundle in a membrane.

(5) N7−*Alm Mutant.* The N7 mutant was constructed by mutating the Q7 residues in the unsolvated bundle using Quanta. This mutated structure was then subjected to a series of minimizations as before. (a) First, the whole bundle was constrained except the Asn residues. (b) Second, harmonic restraints were imposed on the protein backbone only. (c) Third, harmonic restraints were placed on the Cα atoms only. (d) Finally, minimization was performed with no restraints at all. The structure was then solvated in the same fashion as described above, and MD was then performed. In the production phase of this run, the potential energy did not stabilize and the pore radius increased, on average, during the first 60 ps of the run. Therefore, a further 100 ps of MD was performed, by which time the potential energy of the system had stabilized and the pore radius was observed to fluctuate about a steady value. Data were therefore collected only from this last 100 ps of simulation.

(6) Conductance Calculations. Pore radius profiles were determined using HOLE (*26*, *27*). HOLE was also used to estimate conductances for the channel by treating the pore as an irregular cylinder filled with an electrolyte with a constant resistivity (*27*). Integration of the resistance along the pore axis and addition of the access resistance at the mouths of the pore give the total resistance, of which G_{max} is the inverse:

$$G_{max} = \left[\frac{\rho}{4R_a} + \sum_{a}^{b}\frac{\rho}{\pi R^2}\,dz + \frac{\rho}{4R_b}\right]^{-1} \qquad (1)$$

where the pore extends from $z = a$ to $z = b$, where R_a and R_b are the radii at the pore mouths, R *is* the radius as a function of z in the pore, and ρ is the resistivity of the electrolyte solution. Note that corrections for diffusion limitation, to be expected at higher voltages, the effects of a potential barrier (*e.g.* ion dehydration), and hindered diffusion of water and of ions within the lumen of the channel are ignored in this simple model (*44*−*46*).

RESULTS AND DISCUSSION

Peptide Synthesis. Several independent syntheses of natural alamethicin employing solution-phase peptide synthesis methods have been reported (*47*−*50*). These were impressive accomplishments since at least two factors made the synthesis particularly difficult. One was the presence of acid-labile Aib−Pro bonds in the sequence, thus severely limiting the use of traditional protection/deprotection strategies (*50*). Second, the peptide coupling of the sterically hindered Aib residue is very inefficient using standard coupling strategies. Alamethicin contains eight Aib residues, so a sequential solid-phase approach can lead to very low overall yields. Recent introduction of new coupling reagents, in particular Fmoc-protected acid fluorides, has dramatically improved the yield of Aib couplings (*16*−*19*, *51*, *52*). Using the base-labile Fmoc group during synthesis and the very acid-labile *o*-chlorotrityl linker for attachment of the peptide to the resin avoids exposing the Aib−Pro bonds to acid.

Solid-phase synthesis of the monomeric peptides Q7−alm and N7−alm using the acid fluoride technique presented no difficulty. Amino acids were converted to acid fluorides using DAST (*21*) and isolated prior to use in SPPS. Although natural alamethicin has an amino alcohol residue (phenylalaninol) at its C-terminal end, and this site has been targeted for C-terminal cross-linking previously (*20*), we felt that a C-terminal carboxylic acid functional group would permit more straightforward dimerization of the peptides. Thus, Q7−alm and N7−alm were synthesized as peptide acids. After HPLC purification, these peptides were activated using HATU and linked using the diamine bis(*N*-3-aminopropyl)-1,7-heptanediamide (BAPHDA). After coupling, dimers were purified using analytical HPLC and the structures were confirmed by electrospray ionization mass spectrometry (ESI-MS) (Figure 2).

The chemical structures of the dimers are shown in Figure 1. Since the peptides are linked at their C termini via normal peptide bonds rather than via the carbamate groups employed previously, the linkage is shorter by two CH_2O groups overall. Since models indicated that the previous linker was longer than necessary to provide a flexible connection between alamethicin helixes in a bundle, we anticipated that the shorter linker would not interfere with helix−helix packing.

Channel-Forming Properties. Q7−alm monomer, Q7−alm dimer, N7−alm monomer, and N7−alm dimer each formed channels readily in membranes of diphytanoylphosphatidylcholine/decane in a solution of 1 M KCl (5 mM BES at pH 6.8). Representative traces of single-channel current recordings made with an applied potential of 160 mV are shown in Figure 3. Inspection of the recordings reveals several obvious features. The monomers (Figure 3B,D) show the characteristic multistep pattern of currents typical of alamethicin-like molecules (*4*). The current levels observed in each case are indicated by horizontal bars; the step sizes increase with the level number (*53*). The Q7 monomer states (Figure 3B) have somewhat longer average lifetimes than those of the N7−alm monomer (Figure 3D). The same difference was observed between des-Aib-Leu Q7−alm and des-Aib-Leu N7 analogues of alamethicin by Molle et al. (*8*). The difference was attributed to less favorable interannular H bonding in the N7 case (see below).

It is immediately evident from Figure 3 that both the Q7 dimers and the N7 dimers form channels with lifetimes considerably longer than those of their corresponding monomers. Thus, the tethering strategy appears to be general; stabilization of conducting states is observed despite changes in the peptide sequence. Stabilization also does not appear to depend critically on the exact structure of the linker. In the present case, monomers are joined via amide bonds to BAPHDA. Previously, native alamethicin was linked via

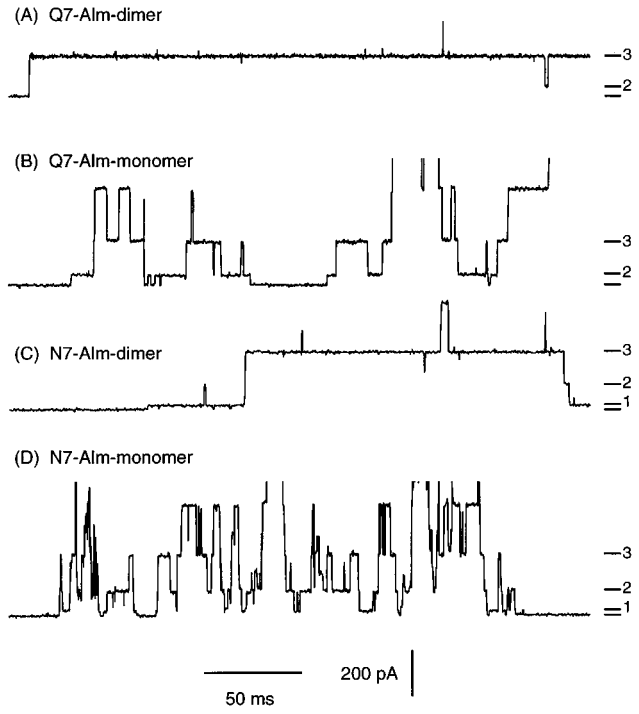

FIGURE 3: Single-channel records of (A) Q7−alm dimer channels, (B) Q7−alm monomers, (C) N7−alm dimers, and (D) N7−alm monomers in 1 M KCl, 5 mM BES (pH 6.8), and diphytanoylphosphatidylcholine with a 160 mV applied voltage. The baseline is the lowest current level in each case, and channels open upward. Current levels are indicated by the horizontal bars at the right. Each monomer−dimer pair exhibits the same pattern of current levels.

carbamate bonds to BAPHDA and another diamine PAPDA (*20*), and a similar stabilization was observed.

This stabilization shows a distinctive pattern; there is selective stabilization of alternate conducting levels. The alternating pattern is evident when one constructs an all-points histogram of times spent in different states for each of the different channel types (Figure 4). The monomeric and dimeric forms of each peptide are compared. In Figure 4A, seven different states are observed for the monomer (Q7). Under these conditions (1 M KCl and 160 mV), level 1 is difficult to distinguish from the baseline, although it is easily observed with higher voltages. The levels are therefore numbered beginning at 2. The channels spend significant amounts of time in all seven states, with state 5 being somewhat preferred. Although the ratios of time spent in these states are rather sensitive to the exact experimental conditions [concentration of peptide, voltage, and salt concentration (*54*)], the behavior of the dimeric form of the peptide is qualitatively different. With the dimer, there are dramatic differences in the fractions of time spent in adjacent states. In Figure 4A, the time the dimer spends in level 2 is vanishingly small compared to the time spent in level 3; similarly, the time spent in level 4 is much less than that spent in level 5. The same pattern is observed with the N7 peptides. In this case, level 1 has a higher conductance and is resolved in the figure. The N7 monomers form channels with six well-populated states. States 1, 3, and 5 are populated by dimer peptides, while states 2, 4, and 6 are not.

This alternating pattern is consistently observed, independent of peptide concentration, voltage, and salt concentration. Indeed, it is evident even from the single-channel recording in Figure 3. Alternate current levels that are well-represented in the recordings of Q7 and N7 monomers appear as only short-lived transitional states in the Q7 and N7 dimer recordings. The most straightforward explanation for these observations is that dimerization selectively stabilizes channel structures containing an even number of alamethicin peptides (*20*).

Conductances of the Q7−Alm Dimer (Level 3) and the N7−Alm Dimer (Level 3). Although dimerization stabilizes particular conducting states, it does not appear to greatly affect the conductance of the different states. The currents associated with the different levels of each monomer−dimer pair are nearly superimposable (Figures 3 and 4). This occurs despite the fact that monomers have ionizable C-terminal carboxyl groups (*i.e.* they may be negatively charged), and dimers are neutral. The N7 dimers and monomers, however, have consistently larger single-channel conductances than the Q7 peptides. This observation is true for all states (1−7) at constant applied voltages.

State 3 (Figures 3 and 4), which is selectively stabilized in both Q7 and N7 dimers, is sufficiently long-lived that a current−voltage relationship may be determined during the lifetime of one conducting channel. Such an $I-V$ curve is shown in Figure 5 for the Q7 dimer, for the N7 dimer, and for the alm−BAPHDA dimer studied previously. The Q7 and alm−BAPHDA $I-V$ curves are superimposable. This result indicates that a very similar conducting structure must be formed by the two peptides despite the difference in the linkers.

For all the constant-voltage recordings (Figure 3) and at the beginning of the voltage ramp shown in Figure 5, alamethicin channels are oriented so that the C-terminal end faces the positive side of the membrane. Cations (K^+) thus enter the C-terminal end of the helix bundle, and Cl^- ions enter the N-terminal end (*55*). As the voltage becomes negative in the single-channel $I-V$ ramp, ions move in the opposite direction. The fact that the observed currents are smaller (Figure 5; *55*) implies that ion movement in this reversed sense (*i.e.* with negative potentials) encounters larger barriers. These barriers have been proposed to be the partial charges at the ends of the peptide helixes (*7, 55−57*).

The N7 dimer level 3 state passes larger currents than the Q7 dimer at positive voltages and nearly equal currents at negative voltages, but the $I-V$ curve has a similar shape (see below).

Structural Interpretation. State 3 is identified as the third level observed above the baseline in both the Q7 and N7 cases. It is selectively stabilized with both peptides. It is thus very likely that state 3 has the same molecularity whether it is formed by Q7 helixes or N7 helixes. The smallest even-numbered helix bundle that can account approximately for the observed conductance of state 3 is a hexamer. Accordingly, we have modeled hexameric versions of both the Q7 dimer and the N7 dimer in an effort to test whether such structures can reasonably account for the observed conductance properties. Hexamer models were built by mutating alm−BAPHDA bundles previously built by simulated annealing via restrained molecular dynamics (*20, 34, 36, 58*) (Figure 6).

We have modeled the bundle as an all-parallel arrangement of helixes because the linkers are too short to permit alternate helixes to be antiparallel without significant distortions in helix packing. Furthermore, the strong voltage dependence of alamethicin channel activation is most easily explained

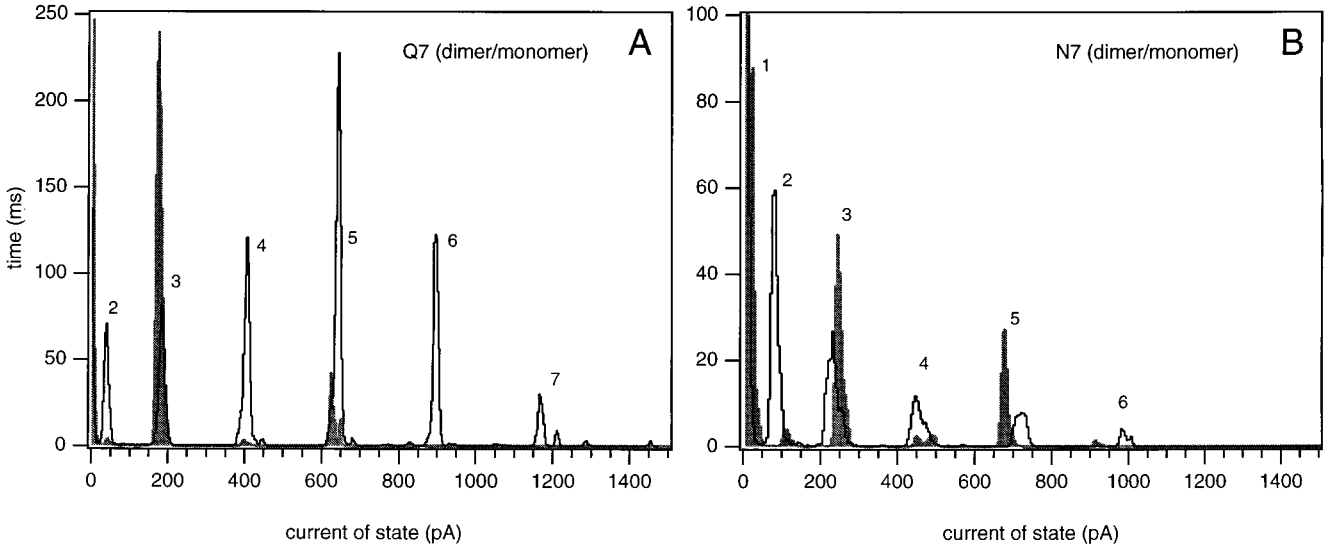

FIGURE 4: All-points histogram of time spent in different current levels for the Q7 dimer−Q7 monomer pair (A) and the N7 dimer−N7 monomer pair (B). The dimer levels are indicated with dark bars and the monomers with an open trace. The current levels are numbered. Channels formed by dimers show an alternating pattern of states; *i.e.* states 2, 4, and 6 are barely populated.

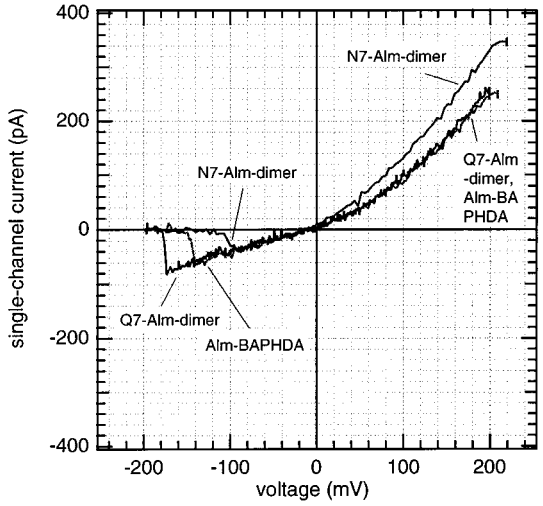

FIGURE 5: Comparison of single-channel $I-V$ curves of state 3 of N7−alm dimer channels, Q7−alm dimer channels, and alm−BAPHDA channels [1 M KCl and 5 mM BES (pH 6.8)]. Channels opened at 200 mV, and the voltage ramp went from 200 to −200 mV.

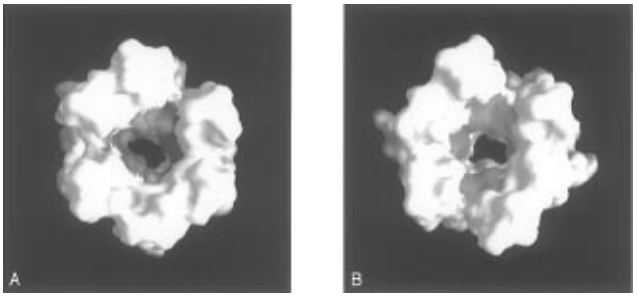

FIGURE 6: GRASP (*61*) surface representations of models of hexameric Q7−alm dimer channels (A) and N7−alm dimer channels (B) viewed from the N-terminal end. Side chain atoms of Gln^7 (A) are colored red, and those of Asn^7 (B) are colored green. The white surface visible behind the green surface in panel B is the constriction formed by the Gln^{18} residues.

in terms of a parallel helix orientation (*2, 33, 41*). However, the possibility that one dimer is oriented differently compared to the other two cannot be completely ruled out (*59*). Other, more complicated models are also possible [*e.g.* multiple conductance pathways (*60*)], but we feel they are not required at this stage to explain the available data.

The dimensions of the pores of these channels can be visualized using the GRASP program (Figure 6), which produces a molecular surface representation of the structure (*61*), and using the HOLE program (Figure 7), which produces a dot surface rendering of the pore lining (*26, 27*). The model channels generated using SA/MD for hexameric Q7 bundles and N7 bundles both show constrictions at the level of the Gln^{18} residues. The Q7 bundle, however, has another clear constriction at the Gln^7 ring, where the Asn^7 bundle has less of a constriction at this site. The lack of a constriction is also evident from time-averaged pore radius profiles calculated using HOLE (Figure 8). The shorter Asn side chain at position 7 results in a channel with a larger (local) diameter. The Q7 bundles shown have structures that permit interhelix H bonding of Q7 side chains (*62*), as originally proposed by Fox and Richards (*63*). The N7 bundles appear to be less well-suited for extensive interhelix H bonding (a factor that may contribute to their shorter average lifetimes), but N7 residues can still make favorable H bonds with water molecules in the pore.

Although it might seem obvious that shortening the side chain at position 7 should result in a larger pore, this result is only expected if the overall bundle structure or the shape of the pore elsewhere does not change as a result of the change at residue 7. Figure 8 shows that the only significant difference in the pore radius between the Q7 and N7 channels occurs in the local vicinity of residue 7. Molle et al. (*8*) have compared the conductances of des-Aib-Leu analogues of the peptides studied here (*i.e.* Q7 des-Aib-Leu and N7 des-Aib-Leu; these peptides also have Glu at position 18, in place of Gln). In that case, the Q7 → N7 change resulted in a decrease in single-channel conductance (for all levels formed by monomers), *i.e.* the opposite of what we observe here. Molle et al. suggest that the Q7 → N7 replacement results in an overall tighter packing of the helixes in the bundle, so that the pore size decreases (*8*). In other words, the Q7 → N7 change is proposed to cause a decrease in the pore radius which would presumably be nonlocal. It is possible that the helix−helix packing of the des-Aib-Leu

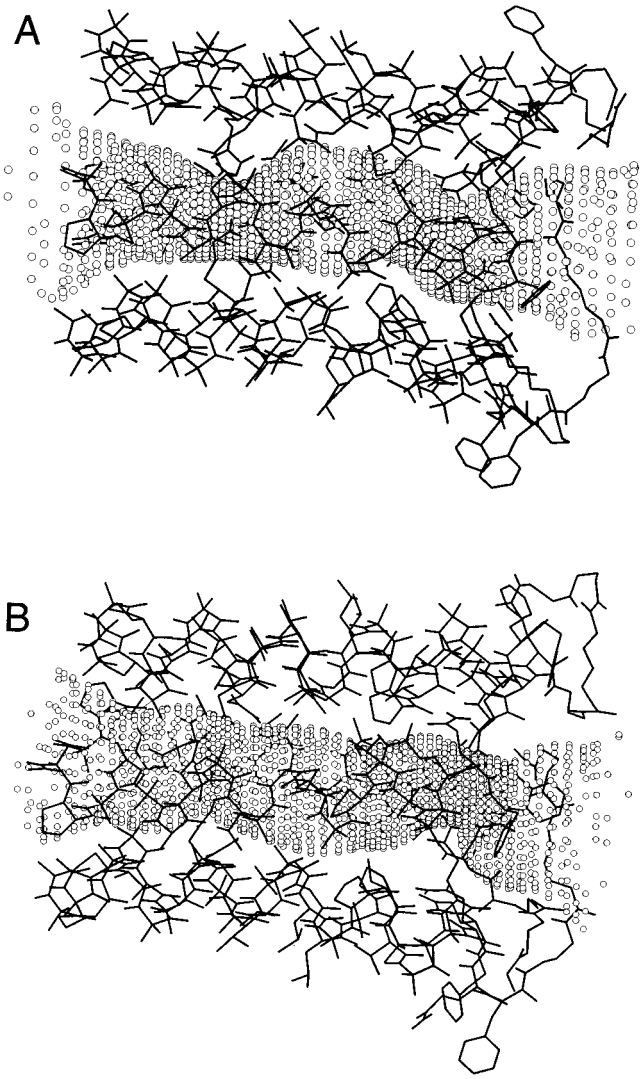

FIGURE 7: Side views of models of the hexameric Q7−alm dimer channel (A) and the N7−alm dimer channel (B). The C terminus is on the right in both cases. The shape of the pore lining as calculated by HOLE (*27*) is represented by rings of circles.

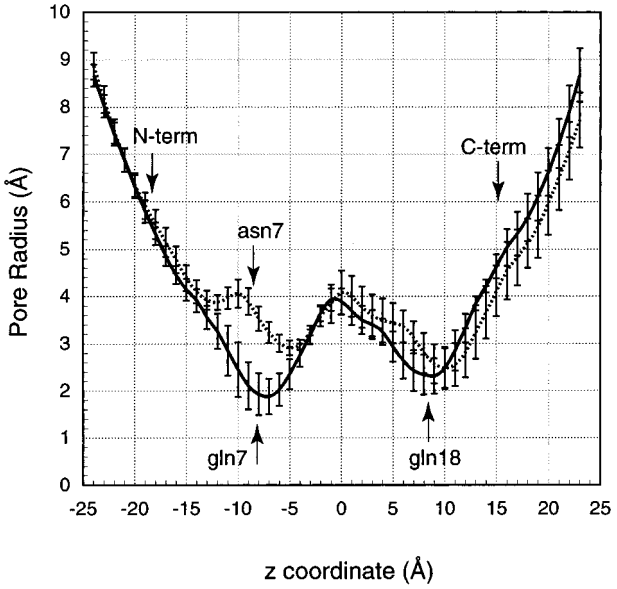

FIGURE 8: Pore radius profiles calculated using HOLE from molecular dynamics simulations of models of hexameric Q7−alm dimer channels and N7−alm dimer channels (see the text for details).

Table 1: Calculated and Experimental Conductances of Q7− and N7−Alm Channels[a]

channel type	predicted conductance (pS)	chord conductance (at 100 mV) (pS)	slope conductance (at 100 mV) (pS)
Q7−alm dimer	810 ± 145	900 ± 100	1300 ± 120
N7−alm dimer	1120 ± 130	1300 ± 100	1700 ± 120

[a] Calculated conductances are uncorrected values obtained using eq 1 in the text and the program HOLE (*27*).

peptides might be perturbed in this way since the geometry of Leu is significantly different from that of Aib (*62*). In the present case, it appears we can consider the Q7 → N7 mutation to be a local structural change. We now consider the consequences of this mutation for the conductance properties of the channels.

It has been argued that, since the current does not saturate with increasing ion concentrations, the alamethicin pore is unlikely to contain distinct binding sites for K^+ or Cl^- (*55, 64*). Thus, conductance changes occurring as a result of a Q7 → N7 mutation will reflect changes in the pore's size, shape, and electrostatic character as well as any changes in access resistance at either end. Since the structural change is local (see above), changes in access resistance are likely to be minor.

The channels are observed to rectify so the conductance depends on the voltage. The $I-V$ curves in Figure 5 show that the conductance of the N7 channels is larger than that of the Q7 channels only with positive voltages. This observation indicates that, with positive voltages, the constriction at Gln^7 is, to some extent, rate-limiting, whereas when cations are entering the N-terminal end of the channel (negative voltages), the Gln^7 constriction has little effect.

If the pore is treated simply as an irregular cylinder with a constant resistivity and corrections for the access resistance are made (see Materials and Methods), the conductance change that would result as a consequence of the increase in the pore diameter with Q7 → N7 can be estimated. Conductances calculated in this way for the Q7 and N7 channels in 1 M KCl are given in Table 1. Experimental slope and chord conductance for ion flow in the normal direction at 100 mV are shown for comparison. Thus, for moderately positive potentials, the increase in conductance with the Q7 → N7 mutation can be reasonably well explained as resulting simply from a larger effective cross-sectional area. This treatment does not explain why there is relatively little difference in conductance at negative voltages.

A more accurate description of ion flow through the pore can be obtained if one employs Nernst−Planck electrodiffusion theory (*65*−*67*). This approach requires one to know, or assume, how the potential experienced by an ion varies with distance along the channel. Electrostatic potentials can be calculated by numerically solving the Poisson−Boltzmann equation as a test charge is moved through the model structure (*33, 55, 68*). The calculated potential profile must then be combined with a description of how the experimentally applied potential varies across the membrane. Using a linear applied field, this approach successfully predicts the rectification observed with alamethicin channels as well as its dependence on ionic strength (*55*). The Q7 → N7 mutation is likely to affect both the calculated electrostatic

potential (due to the channel environment) and the shape of the applied field. A full description of the conductance properties of the system must therefore await the further developments of these theories of permeation. Qualitatively, however, it appears the Q7 → N7 mutation, *i.e.* a local widening of the pore, may or may not result in increased ion flux depending on the relative magnitude of other barriers to permeation (for instance the partial charges at the ends of the peptide helixes). The role of these other barriers, in turn, depends on the particular value of the applied potential.

In summary, the residue at position 7 has a distinct effect on the stability of alamethicin helix bundles and their conductance, under specific experimental conditions (1 M KCl, with diphytanoylphosphatidylcholine/decane membranes). Changes at the C-terminal end, on the other hand, have little effect on conductance under the same conditions, although tethering clearly stabilizes particular channel states. The combined approach of chemical synthesis, molecular modeling, and single-channel analysis, thus, can permit a systematic investigation of the dependence of the conductance properties of a prototype helix-bundle channel on the molecular structure of the pore lining.

REFERENCES

1. Cafiso, D. S. (1994) *Annu. Rev. Biophys. Biomol. Struct. 23*, 141−165.
2. Woolley, G. A., and Wallace, B. A. (1992) *J. Membr. Biol. 129*, 109−136.
3. Akerfeldt, K. S., Lear, J. D., Wasserman, Z. R., Chung, L. A., and DeGrado, W. F. (1993) *Acc. Chem. Res. 26*, 191−197.
4. Latorre, R., and Alvarez, O. (1981) *Physiol. Rev. 61*, 77−150.
5. Sansom, M. S. P. (1993) *Eur. Biophys. J. 22*, 105−124.
6. Unwin, N. (1995) *Nature 373*, 37−43.
7. Lear, J. D., Schneider, J. P., Kienker, P. K., and DeGrado, W. F. (1997) *J. Am. Chem. Soc. 119*, 3212−3217.
8. Molle, G., Dugast, J. Y., Spach, G., and Duclohier, H. (1996) *Biophys. J. 70*, 1669−1675.
9. Duclohier, H., Molle, G., and Spach, G. (1989) in *Peptides 1988*, pp 357−359, Walter de Gruyter & Co., Berlin.
10. Duclohier, H., Molle, G., Dugast, J., and Spach, G. (1992) *Biophys. J. 63*, 868−873.
11. Molle, G., Duclohier, H., and Spach, G. (1987) *FEBS Lett. 224*, 208−212.
12. Molle, G., Dugast, J., Duclohier, H., and Spach, G. (1988) *Biochim. Biophys. Acta 938*, 310−314.
13. Molle, G., Duclohier, H., Dugast, J. Y., and Spach, G. (1989) *Biopolymers 28*, 273−284.
14. Molle, G., Duclohier, H., Julien, S., and Spach, G. (1991) *Biochim. Biophys. Acta 1064*, 365−370.
15. Molle, G., and Dugast, J. Y. (1990) *Tetrahedron Lett. 31*, 6355−6356.
16. Kaduk, C., Duclohier, H., Dathe, M., Wenschuh, H., Beyermann, M., Molle, G., and Bienert, M. (1997) *Biophys. J. 72*, 2151−2159.
17. Carpino, L. A., Beyermann, M., Wenschuh, H., and Bienert, M. (1996) *Acc. Chem. Res. 29*, 268−274.
18. Wenschuh, H., Beyermann, M., Krause, E., Brudel, M., Winter, R., Schumann, M., Carpino, L. A., and Bienert, M. (1994) *J. Org. Chem. 59*, 3275−3280.
19. Wenschuh, H., Beyerman, M., Haber, H., Seydel, J. K., Krause, E., and Bienert, M. (1995) *J. Org. Chem. 60*, 405−410.
20. You, S., Peng, S., Lien, L., Breed, J., Sansom, M. S. P., and Woolley, G. A. (1996) *Biochemistry 35*, 6225−6232.
21. Kaduk, C., Wenschuh, H., Beyermann, M., Forner, K., and Carpino, L. A. (1996) *Lett. Pept. Sci. 2*, 285−288.
22. Seoh, S., and Busath, D. (1993) *Biophys. J. 64*, 1017−1028.
23. Brunger, A. T. (1993) *X-PLOR, Version 3*, Yale University Press, New Haven, CT.
24. Brooks, B. R., Bruccoleri, R. E., Olafson, B. D., States, D. J., Swaminathan, S., and Karplus, M. (1983) *J. Comput. Chem. 4*, 187−217.
25. Kraulis, P. J. (1991) *J. Appl. Crystallogr. 24*, 946−950.
26. Smart, O. S., Goodfellow, J. M., and Wallace, B. A. (1993) *Biophys. J. 65*, 2455−2460.
27. Smart, O. S., Breed, J., Smith, G. R., and Sansom, M. S. P. (1997) *Biophys. J. 72*, 1109−1126.
28. Nilges, M., and Brunger, A. T. (1991) *Protein Eng. 4*, 649−659.
29. Nilges, M., and Brunger, A. T. (1993) *Proteins 15*, 133−146.
30. Sankararamakrishnan, R., and Sansom, M. S. P. (1995) *Biophys. Chem. 55*, 215−230.
31. Sankararamakrishnan, R., and Sansom, M. S. P. (1994) *Biochem. Soc. Trans. 22*, 156S.
32. Kerr, I. D., Son, H. S., Sankararamakrishnan, R., and Sansom, M. S. P. (1996) *Biopolymers 39*, 503−515.
33. Breed, J., Biggin, P. C., Kerr, I. D., Smart, O. S., and Sansom, M. S. P. (1997) *Biochim. Biophys. Acta 1325*, 235−249.
34. Kerr, I. D., Sankararamakrishnan, R., Smart, O. S., and Sansom, M. S. P. (1994) *Biophys. J. 67*, 1501−1515.
35. Kerr, I. D., and Sansom, M. S. P. (1996) *Biochem. Soc. Trans. 24*, 297S.
36. Breed, J., Kerr, I. D., Sankararamakrishnan, R., and Sansom, M. S. P. (1995) *Biopolymers 35*, 639−655.
37. Sankararamakrishnan, R., and Sansom, M. S. P. (1995) *Biochim. Biophys. Acta 1239*, 122−132.
38. Mitton, P., and Sansom, M. S. P. (1996) *Eur. Biophys. J. 25*, 139−150.
39. Breed, J., Sankararamakrishnan, R., Kerr, I. D., and Sansom, M. S. P. (1996) *Biophys. J. 70*, 1643−1661.
40. Jorgensen, W. L., Chandresekhar, J., Madura, D., Impey, R. W., and Klein, M. L. (1983) *J. Chem. Phys. 79*, 926−935.
41. Biggin, P. C., Breed, J., Son, H. S., and Sansom, M. S. P. (1997) *Biophys. J. 72*, 627−636.
42. Biggin, P. C., and Sansom, M. S. P. (1996) *Biochem. Soc. Trans. 24*, 137S.
43. Gazit, E., Miller, I. R., Biggin, P. C., Sansom, M. S. P., and Shai, Y. (1996) *J. Mol. Biol. 258*, 860−870.
44. Laver, D. R. (1994) *Biophys. J. 66*, 355−359.
45. Kuyucak, S., and Chung, S. H. (1994) *Biophys. Chem. 51*, 15−24.
46. Sansom, M. S. P., and Kerr, I. D. (1995) *Biophys. J. 69*, 1334−1343.
47. Balasubramanian, T. M., Kendrick, N. C. E., Taylor, M., Marshall, G. R., Hall, J. E., Vodyanoy, I., and Reusser, F. (1981) *J. Am. Chem. Soc. 103*, 6127−6132.
48. Gisin, B. F., Davis, D. G., Borowska, Z. K., Hall, J. E., and Kobayashi, S. (1981) *J. Am. Chem. Soc. 103*, 6373−6377.
49. Nagaraj, R., and Balaram, P. (1981) *Tetrahedron 37*, 1263−1270.
50. Schmitt, H., and Jung, G. (1985) *Liebigs Ann. Chem.*, 321−344.
51. Barranger-Mathys, M., and Cafiso, D. S. (1996) *Biophys. J. 35*, 498−505.
52. Carpino, L. A. (1993) *J. Am. Chem. Soc. 115*, 4397−4398.
53. Sansom, M. S. P. (1993) *Q. Rev. Biophys. 26*, 365−421.
54. Woolley, G. A., Epand, R. M., Kerr, I. D., Sansom, M. S. P., and Wallace, B. A. (1994) *Biochemistry 33*, 6850−6858.
55. Woolley, G. A., Biggin, P. C., Schultz, A., Lien, L., Jaikaran, D. C. J., Breed, J., Crowhurst, K., and Sansom, M. S. P. (1997) *Biophys. J. 73*, 770−778.
56. Kienker, P. K., Degrado, W. F., and Lear, J. D. (1994) *Proc. Natl. Acad. Sci. U.S.A. 91*, 4859−4863.
57. Kienker, P. K., and Lear, J. D. (1995) *Biophys. J. 68*, 1347−1358.
58. Breed, J., and Sansom, M. S. P. (1994) *Biochem. Soc. Trans. 22*, 157S.
59. Mak, D. D., and Webb, W. W. (1995) *Biophys. J. 69*, 2323−2336.
60. Bezrukov, S. M., and Vodyanoy, I. (1993) *Biophys. J. 64*, 16−25.

61. Nicholls, A. J. (1993) *GRASP: Graphical Representation and Analysis of Surface Properties*, Columbia University, New York.
62. Breed, J. (1996) Molecular Modelling of Ion Channels, Ph.D. Thesis, University of Oxford, Oxford, England.
63. Fox, R. O., Jr., and Richards, F. M. (1982) *Nature 350*, 325−330.
64. Haydon, D. A., Hladky, S. B., and Gordon, L. G. M. (1972) in *Mitochondria: biogenesis and bioenergetics. Biomembranes: molecular arrangements and transport mechanisms.* (van den Bergh, S. G., Ed.) pp 307−316, North-Holland, Amsterdam.
65. Arndt, R. A., and Roper, L. D. (1972) *Simple Membrane Electrodiffusion Theory*, Physical Biological Sciences Misc., Blacksburg, VA.
66. Schultz, S. G. (1980) *Basic Principles of Membrane Transport*, Cambridge University Press, Cambridge, England.
67. Hille, B. (1992) *Ionic Channels of Excitable Membranes*, 2nd ed., Sinauer, Sunderland, MA.
68. Sankararamakrishnan, R., Adcock, C., and Sansom, M. S. P. (1996) *Biophys. J. 71*, 1659−1671.

BI9716130